Research Square

Preprints are preliminary reports that have not undergone peer review.
They should not be considered conclusive, used to inform clinical practice,
or referenced by the media as validated information.

Feasibility Verification and Electrical Performance of Additive-manufactured Flexible Microspiral Inductor Made of Copper Wire

Wenjie Niu (wenjie_niu@163.com)
China University of Petroleum Huadong https://orcid.org/0000-0003-1225-1467
Mengxue Yang
China University of Petroleum Huadong
Yu Gong
China University of Petroleum Huadong
Yu Liu
China University of Petroleum Huadong
Yanfang Zhang
Tianjin Sanying Precision Instruments

Research Article

Keywords: Flexible electronics, Microspiral inductor, Copper wire, Numerical simulation, Electrical performance characterization

Posted Date: May 31st, 2022

DOI: https://doi.org/10.21203/rs.3.rs-1118271/v1

License: This work is licensed under a Creative Commons Attribution 4.0 International License.
Read Full License

Abstract

In recent years, flexible electronic technology has been rapidly developed. Compared with common conductive materials, copper wire has the advantages of high conductivity and low cost. To verify the feasibility of fine copper wire as the conductive material in flexible microelectronic components, a microspiral inductor was taken as an example in this work. First, flexible passive microspiral inductors with 2.5, 4.5, and 6.5 turns were prepared by injection molding using the stereo lithography (SLA) technology to print a mold, with silicone rubber (Ecoflex) as the base material and copper wire as the conductive material. Second, theoretical models of the flexible microspiral inductors with different turns were numerically simulated, and physical experiments on the electrical performance of actual microspiral inductors were conducted under initial and deformation states. The two results were then compared and analyzed. The results showed that the maximum errors in the inductance, quality factor, and self-resonant frequency in the initial state were +18.17%, −19.33%, and 0.17 GHz, and those in the deformation state were +11.15%, −10.88%, and 0.09 GHz. The errors were no more than 20%. These results confirm the feasibility of using copper wire as the conductive material in flexible electronic components.

1. Introduction

In recent years, with the rapid development of electronic technology, microelectronic components, such as resistors, capacitors, and inductors, are being increasingly used in various fields [1]. Flexible electronic technology is a new type of electronic technology, whereby organic or microelectronic devices can be prepared on flexible, plastic, or thin surfaces. Flexible electronic components are composed of high-ductility base materials and embedded conductive materials. With their unique flexibility, ductility, high efficiency, and low-cost manufacturing process, flexible electronics have a wide application prospect in the fields of information, energy, medical treatment, and national defense [2–5]. They have unique applications in passive radio frequency [6–8], additive manufacturing (AM) technology [9, 10], and health monitoring [11–13]. Highly malleable elastic materials can protect devices and interconnects from large-scale deformation and corrosive environments [14, 15]. Therefore, they are often used in the fabrication of flexible antennas, hydrogels, and sensors [16–20].

The combination of flexible electronics and AM technology is an emerging and important research direction. Flexible microelectronic components printed directly using the AM technology are easily affected by the printing accuracy of the printer, produce defects, and have a low degree of deformation [21]. Some flexible wearable products embedded with microsensors can be prepared by embedding conductive materials into flexible base materials through an embedded 3D printing process [22, 23]. However, the process parameters of the AM and the damage induced in the process of material delamination may lead to various types of dimensional deviations and internal defects, affecting the manufacturing quality and material performance. Lazarus et al. used the 3D printing technology to prepare a mold, established a flexible inductance structure of a biplane coil and 3D spiral, and conducted tensile and compressive strain tests [24, 25]. Currently, research on the fabrication of flexible microelectronic components using AM is limited to 2D cases, with little research on 3D passive

components and the influence of parameter variation and deformation degree of a material on its electrical properties [26].

A liquid metal has good fluidity and machinability at room temperature. It is a conductive material commonly used in laboratories to prepare microflexible electronic components [27]. Zhou et al. and Amir et al. developed an ink formed by combining a liquid metal and an organic matter and printed it directly onto a base material to prepare flexible electronic products [28, 29]. However, because of the diffusion of the ink between the surface or stacking layers, the pores generated during printing may lead to electrical cut-out [30, 31]. Injecting a liquid metal into the microchannels of a substrate material is another common method of fabricating flexible electronic components. Eutectic gallium indium (EGaIn) is an alloy composed of gallium and indium mixed in the ratio of 3:1. It is nontoxic and has a low viscosity and better electrical conductivity than other liquid metals such as Galinstan (a eutectic alloy composed of gallium, indium, and tin). Owing to this property, EGaIn has recently been used to manufacture flexible antennas [32, 33], sensors [34], multiaxis Helmholtz coils [26], and passive coils [24, 25]. However, when exposed to air at room temperature, EGaIn forms a thin white gallium oxide layer, which limits the free movement of the liquid metal to a certain extent [26]. Moreover, the direct injection of the liquid metal will leave a gap in the die cavity, thus reducing the conductivity. Spraying silica nanoparticles or low-concentration NaOH solution on the base material can help improve the contact angle between EGaIn and the channel [35, 36]. However, the liquid leakage due to EGaIn injection, excessive pressure in the channel, and high requirements for the inner diameter of the injected pinhole continue to affect the performance of micropassive components.

Copper has the advantages of good conductivity and thermal conductivity, and strong fatigue resistance. Currently, studies on the fabrication of micropassive electronic components with copper as the conductive material are lacking. Conventional technical routes, such as thick copper process or copper single Damascene process, can be used to produce planar spiral inductors [37, 38]; however, it is difficult to produce flexible micropassive components through this process. The commonly used screen printing technology, substrate-assisted electrochemical deposition (SAED) technology, and inkjet technology can be used to prepare flexible micropassive components with copper as the conductive material to a certain extent [39–41]; however, the manufacturing process is complex, and the cost of copper film and copper nanoparticles as the conductive material is high. Copper wire as a conductive material has a low cost and a simple manufacturing process. Currently, there are no studies on the electrical properties of flexible electronic components with copper wire as the conductive material. Therefore, the overall capability of this method is yet to be fully evaluated.

In this work, we selected a microspiral inductor, one of the components of an LC passive wireless sensor, as the research object to study and analyze the feasibility of copper wire as the conductive material for the flexible microelectronic element. First, the base material and conductive material of the microspiral inductor were selected, and a microspiral inductor was fabricated. Second, a theoretical model of the spiral inductor was numerically simulated, and the electrical properties and physical experiments of the

spiral inductor in the initial and deformation states were conducted. Finally, the results were compared and analyzed, from which relevant conclusions are drawn.

2. Materials And Fabrication

2.1 Material properties and comparison

To make high-performance flexible passive components, the selection of the base and conductive materials has been an important research direction. Elastic base materials mainly include carbon nanotubes (CNTs), zinc oxide, graphene, semiconductor oxides, and other materials. Among them, semiconductor oxides, such as polydimethylsiloxane (PDMS), silicone rubber (Ecoflex), and polyurethane (PU), are widely used. They have the advantages of low cost, transparency, and surface hydrophobicity [42]. Table 1 presents a comparison between Ecoflex and PDMS in terms of their material properties. The comparison shows that the Young's modulus of Ecoflex is low, and its elastic modulus matches the elastic modulus of human skin, making it a favorable base material for practical bonding applications. Therefore, Ecoflex 00-50 material was selected as the base material of the flexible micropassive spiral inductor.

Table 1
Performance comparison of Ecoflex and PDMS substrate materials

Materials	Tensile strength (MPa)	Maximum strain (%)	Young's modulus (MPa)
Ecoflex 00-50	1.38	900	0.07
PDMS	6.25	120–160	2.05

The selected Ecoflex (BASF Company, Germany) has good tensile properties and can be made with a film thickness of 10 μm. It has good barrier performance to oxygen and water vapor, and it is a common material used in elastic electrodes and flexible sensors [43]. Ecoflex comprises Parts A and B (as shown in Fig. 1 (a)). When in use, it should be mixed and solidified in the ratio of 1:1 at room temperature to form a solid. It is typically necessary to manufacture the mold through the AM technology and then make the required shape through an injection molding process. Compared with the fused deposition modeling (FDM) technology, the stereo lithography (SLA) technology in AM has the advantages of high molding accuracy and good processing quality. In this work, an SLA printer (shown in Fig. 1 (c)) (model Z Rapid SL500; ZRapid Technologies, Suzhou, China) and a photosensitive resin material were first selected to manufacture the mold. Fig. 1 (b) shows the final mold.

The coil and wire diameters of the copper wire, which is the conductive material in flexible electronic components, cannot be changed by stretching and bending compared with EGaIn, whereas its inductance can be changed by changing the pitch and pitch diameter. Table 2 presents a performance comparison between EGaIn and copper wire as conductive materials. Therefore, for some flexible sensors that require

a high inductance performance and small inductance change, using copper wire as a conductive material has the advantages of simple production process, low cost, and high conductivity. Through a tensile test, it is found that, the greater the wire diameter, the lower the change in the pitch and pitch diameter of the microspiral inductor during deformation. Therefore, a copper wire with a diameter of 0.2 mm was selected as the conductive material. Through experimental measurement, the conductivity of the copper wire selected in this study was found to be 1.1247×10^7 S/m. The microspiral inductor was modeled, designed, and manufactured. Fig. 1 (d) (top) shows the theoretical model.

Table 2
Comparison between liquid metal EGaIn and copper wire as conductive materials in terms of their properties

Conductive material	**EGaIn**	**Copper wire**
Component	A eutectic alloy in which gallium and indium are mixed in a ratio of 3:1	Cu + Ag≥99.90
Relative permeability	0.9999	0.999991
Conductivity (S/m)	3.4×10^6	Up to 5.8×10^7
Cost	High	Low
Production process	Complex	Simple
Packaging difficulty	High, prone to liquid metal overflow	Low

2.2 Manufacturing process

The manufacturing process of the flexible microspiral inductor used in this work is as follows:

Step 1: Use the AM technology to manufacture molds. The molds are printed using an SLA 3D printer with a photosensitive resin to prepare the base materials and soft cores convenient for copper wire winding;

Step 2: Mix Parts A and B of Ecoflex 00-50 in the ratio of 1:1 and stir evenly (as shown in Fig. 2 (a)), inject them into the two molds through a 2.5 ml syringe, and cure at room temperature for approximately 3 h;

Step 3: After curing, remove the Ecoflex from the mold to obtain the base groove and soft core of the Ecoflex material (as shown in Fig. 2 (b));

Step 4: Wind the copper wire with a diameter of 0.2 mm on the soft core to form 2.5, 4.5, and 6.5 turns of copper wire coils;

Step 5: Place the wound copper wire coil in the cured concave Ecoflex groove and continue to inject Ecoflex. After the copper wire is completely covered, cure it at room temperature for approximately 3 h to obtain flexible microspiral inductors with different turns (as shown in Fig. 2 (c)).

Fig. 1 (d) (bottom) shows the final sample of the microspiral inductor.

3. Results And Discussion Of Numerical Simulation

To confirm whether the flexible microspiral inductor made of copper wire meets the variation law and design requirements of general inductors, it is necessary to discuss the changes in the inductance value L, quality factor Q (Q factor), and self-resonant frequency (f_{SRF}) under static and deformation states. The inductance value reflects the ability of the inductor to convert electric energy into magnetic energy; the Q factor represents the efficiency with which the inductor converts electric energy into magnetic energy and reflects the loss of the inductor. The self-resonant frequency directly determines the upper frequency limit of the normal operation of the inductor. In this work, the simulation method and physical experiment method were employed, and the measured results were compared and analyzed.

The electrical performance of the flexible microspiral inductor was simulated using Ansys HFSS (high-frequency structure simulator) to analyze the variation in its electrical performance with the frequency. By establishing the simulation model in HFSS and setting the corresponding parameters, such as the frequency, excitation source, radiation boundary, and accuracy, the simulation results, such as the admittance, inductance value, and Q factor, could be obtained. The solution process mainly comprises the following steps:

Step 1: Use SolidWorks software to model the microspiral inductors with 2.5, 4.5, and 6.5 turns. Taking the copper wire with 4.5 turns as an example, the specific modeling parameters are shown in Table 3. The model is then saved in the “x_t” format in the HFSS, and the material properties are defined.

Step 2: Set boundary conditions. In this work, the boundary condition is set as radiation boundary.

Table 3
Specific parameters of microspiral inductor modeling

Turns	Wire diameter (mm)	Coil diameter (mm)	Pitch (mm)	Coil length (mm)	Inductor dimensions (mm)
2.5	0.2	5	3	10.5	40×20×7.5
4.5	0.2	5	3	16.5	
6.5	0.2	5	3	22.5	

Step 3: Set the excitation port. In this work, the lumped port is used as the excitation mode, and the integral line with the same direction is defined.

Step 4: Set solution value and mesh. The frequency scanning range set in this work is 0–1 GHz, the step size is 0.05 GHz, and the frequency scanning type is “Discrete.” The adaptive meshing function in the HFSS is used for meshing.

Step 5: Simulation solution. Based on the settings of the above parameters, the “Analyze ALL” mode is used to complete the simulation solution. The complexity of the spiral inductor geometric model, the setting of the solution value, the division of the network, and the configuration of the computer influence the simulation time.

When using the HFSS for electrical simulations, the calculation formulae for the inductance (Equation (1)) and Q factor (Equation (2)) are as follow:

$$L = \mathrm{Im}(1/Y_{11})/(2*\pi*Freq) \quad (1)$$

$$Q = \frac{\mathrm{Im}(1/Y_{11})}{\mathrm{Re}(1/Y_{11})} \quad (2)$$

Here, Y_{11} is the admittance, *Freq* is the operating frequency, *Im* refers to the imaginary part of $1/Y_{11}$, and *Re* refers to the real part of $1/Y_{11}$.

For the microspiral inductors with 2.5, 4.5, and 6.5 turns, this work simulates the inductance value and Q factor in its initial state (unstressed). Figures 3 (a) and (b) show the simulation results. As shown, with the increase ofin the number of inductor turns, the inductance increases; however, it will also lead to an increase in the parasitic capacitance and a decrease in the Q factor. The stray capacitance increases with the increase in the number of turns, thereby decreasing f_{SRF}.

For the 4.5-turn microspiral inductor, the inductance and Q factor in the initial state, deformation state 1 (the length after stretching is 50 mm), and deformation state 2 (the length after stretching is 70 mm) were simulated. Figures 3 (c) and (d) show the simulation results. With the deformation of the flexible inductor, the pitch of the copper wire increases, which reduces the mutual inductance between the coils, thereby reducing the total inductance; however, increasing the pitch reduces the parasitic capacitance and eddy current loss of the coil, thus increasing the Q factor.

Table 4
Numerical simulation results of various parameters of the microspiral inductor under different turns and deformation states

Turns	2.5	4.5	6.5	4.5 (Deformation state 1)	4.5 (Deformation state 2)
Maximum inductance value (nH)	993.11	1509.84	1762.69	1406.89	1197.72
Maximum Q factor	82.43	69.13	61.66	71.34	77.14
f_{SRF} (GHz)	0.39	0.45	0.48	0.38	0.44

Table 4 presents the specific data of the simulation results. From the simulation results, the changes in the inductance and Q factor with the increase in the number of turns and tensile properties of the flexible microspiral inductor are in agreement with the change law of the general flexible inductor. The results are suitable to determine the electrical performance in the subsequent experiment.

4. Results And Discussion Of Electrical Performance

4.1 Electrical performance experiment

The numerical simulation is an electrical performance simulation conducted on the microspiral inductor in the ideal state. For flexible microspiral inductors manufactured with a thin copper wire as the conductive material and AM technology, an electrical performance experiment should be conducted to evaluate the influence of manufacturing process, material performance, and other factors on its performance.

First, this study uses the SolidWorks software to design a fixture that can measure the inductance and Q factor under deformation, as shown in Fig. 4. Figure 4 (a) shows the SolidWorks model of the fixture, which is composed of a fixed part, a moving part, and a screw. The fixed part is connected using the screw in the form of a slot, and the moving part is connected using the screw in the form of a thread. Figures 4 (b) and (c) show the fixture printed using the AM technology. When in use, the two sides of the microspiral inductor (as shown in Fig. 4 (d)) are clamped, the clamp is nested in the two cylinders of the fixed and moving parts, and the distance between the moving and fixed parts is adjusted by rotating the screw. This helps achieve the objectives of stretching and deformation of the microspiral inductor. Figures 4 (e) and (g) show the deformation degree of the flexible microspiral inductor in the initial state, deformation state 1, and deformation state 2.

The impedance analyzer can measure the reactance and inductive reactance of the impedance varying with the frequency and then convert them into the inductance value and Q factor. In this work, the Agilent E4991A impedance analyzer was selected to test the electrical performance of the manufactured microspiral inductor, and the inductance and Q factor of the microspiral inductor in the frequency range of 0–2 GHz were obtained (as shown in Fig. 5).

For inductors, the expressions of L and Q are:

$$\begin{cases} L = \dfrac{X}{2\pi f} \\ Q = \dfrac{X}{R} \end{cases} \quad (3)$$

where the resistance R is the real part of the impedance Z, the inductive reactance X is the imaginary part of the impedance Z, and f is the frequency.

For the microspiral inductors with 2.5, 4.5, and 6.5 turns, the inductance and Q factor in the initial state were tested. Figures 6 (a) and (b) show the experimental results. In addition, to verify the electrical performance under deformation, the inductance and Q factor of the 4.5-turn microspiral inductor in the initial state, deformation state 1, and deformation state 2 are tested, as shown in Figs. 6 (c) and (d).

Table 5
Experimental detection results of various parameters of the microspiral inductor under different turns and deformation states

Turns	**2.5**	**4.5**	**6.5**	**4.5 (Deformation state 1)**	**4.5 (Deformation state 2)**
Maximum inductance value (nH)	1112.10	1698.12	1982.02	1563.72	1233.66
Maximum Q factor	89.64	60.54	49.74	63.58	70.86
f_{SRF} (GHz)	0.41	0.32	0.31	0.33	0.35

Table 5 presents the specific data of the physical experiment results. From the experimental results, the variation in the inductance and Q factor with the increase in the number of turns and the variation trend in the tensile properties of the flexible microspiral inductor are in accordance with the variation law of general flexible inductors. However, a further analysis and comparison with the numerical simulation results are still required.

4.2 Comparison and analysis

Figure 7 shows a comparison between the physical experimental results and the numerical simulation results under the initial state of the 2.5-, 4.5-, and 6.5-turn flexible microspiral inductors and the deformation state of the 4.5-turn microspiral inductor.

The figure shows that the physical experimental results of the inductance L and Q factor of the flexible microspiral inductor based on the AM technology are roughly the same as the numerical simulation results of the theoretical model. The change rates of the inductance are +11.98%, −1.3%, +18.17%, +11.15%, and +3%. The change rates of the Q factor are + 8.75%, −12.42%, −19.33%, −10.88%, and −8.15%. The changes in the self-resonant frequency are 0.02, 0.13, 0.17, 0.05 and 0.09, as listed in Table 6.

Table 6
Comparison between the physical experiment results and numerical simulation results

Number of turns	Errors		
	Inductance	Q factor	f_{SRF}
2.5	+11.98%	+8.75%	0.02
4.5	−1.3%	−12.42%	0.13
6.5	+18.17%	−19.33%	0.17
4.5 (Deformation state 1)	+11.15%	−10.88%	0.05
4.5 (Deformation state 2)	+3%	−8.15%	0.09

The relatively large error is mainly reflected in the following two aspects:

1. The physical experiment results of f_{SRF} are earlier than those of the numerical simulation results.
2. The change rate of the individual inductance and Q factor is slightly higher.

The main reasons for the difference between the physical experiment results and numerical simulation results are as follows:

(1) Differences in material parameters. In the actual manufacturing process of a microspiral inductor, the actual working performance index of the material deviates from the specified theoretical value. Specifically, the impurities with little content in copper, particularly phosphorus, arsenic and aluminum, or

a small amount of oxygen easily mixed during copper smelting, have a significant impact on the conductivity. Moreover, there is a difference between the increase rate of the actual resistance and that of the theoretical simulation.

(2) There are geometric parameter errors between the actual microspiral inductor and the expected model. Specifically, the limitations of the AM technology in manufacturing molds, injection molding process of the silicon rubber, and manufacturing of the microspiral inductors will lead to dimensional errors between the different components of the microspiral inductors.

(3) Parasitic effects of actual devices. The parasitic effect of the actual device may be greater than the theoretically simulated value, and the dielectric constant of the insulating material is also different at different frequencies.

In conclusion, a passive microspiral inductor with copper wire as the conductive material for the flexible passive components exhibits roughly the same change trend in terms of the physical experiment and numerical simulation results. Moreover, it meets the electrical change law of general flexible passive components in terms of the tensile properties.

5. Conclusion And Prospect

In this work, to verify the feasibility of fine copper wire as the conductive material in flexible microelectronic components and to study the corresponding electrical properties, a microspiral inductor was taken as an example. A mold was manufactured using the SLA technology, a flexible substrate was processed by silicon rubber injection molding, and a flexible micropassive inductor was prepared using copper wire instead of EGaIn. The electrical performance was simulated using Ansys HFSS and Agilent E4991A impedance analyzer. The results showed that the variation trend in the physical experiment results is roughly the same as that in the numerical simulation results of the theoretical model. The errors in the inductance values were +11.98%, −1.3%, +18.17%, +11.15%, and +3%. The errors in the Q factor were +8.75%, −12.42%, −19.33%, −10.88%, and −8.15%. The errors in f_{SRF} were 0.02, 0.13, 0.17, 0.05, and 0.09 GHz. The error was mainly reflected in the fact that f_{SRF} of the inductance was earlier than that of the numerical simulation, and the change rate of the individual inductance and Q factor was slightly higher. The main reasons were the difference in the material parameters and the dimensional error of the geometric model. It is concluded that the tensile performance of the flexible passive inductor manufactured in this work meets the electrical variation law of general flexible passive components, with the error being no more than 20%, thus proving the feasibility of using copper wire as the conductive material in flexible passive components.

This work only tested copper wire as the conductive material. For different materials of the copper wire, such as brass, bronze, and red copper, and different models of the copper wire, such as TU1, TU2, TUP, and other models, as conductive materials, relevant numerical analysis and experimental verification

should be performed in the future. The deformation degree and electrical properties of copper wire with a diameter of more than 0.2 mm and low deformation should be further studied experimentally.

Declarations

Funding

This research received no external funding.

Conflict of Interest

The authors declare no conflict of interest.

References

1. Wu, S. Y., Yang, C., Hsu, W., Lin, L.: 3D-printed microelectronics for integrated circuitry and passive wireless sensors. Microsyst. Nanoeng. 1, 15013 (2015)
2. Ready, S., Whiting, G., Ng, T. N.: Multi-material 3D printing. In NIP & Digital Fabrication Conference, 2014 International Conference on Digital Printing Technologies. 120–123 (2014)
3. Vatani, M., Lu, Y., Engeberg, E. D., Choi, J. W.: Combined 3D printing technologies and material for fabrication of tactile sensors. Int J Precis Eng Man. 16, 1375–1383 (2015)
4. Zhao, Y., Xian, H.: Mechanisms and Materials of Flexible and Stretchable Skin Sensors. Micromachines. 8, 69 (2017)
5. Corzo, D., Tostado, B. G., Baran, D.: Flexible Electronics: Status, Challenges and Opportunities. Frontiers in Electronics. (2020)
6. Zhou, N., Liu, C., Lewis, J. A., Ham, D.: Gigahertz electromagnetic structure via direct ink writing for radio-frequency oscillator and transmitter application. Adv. Mater. 29 (2017)
7. Wu, S. Y., Lin, C. C., Lin, D. Y., Chen, A. L., Liu, S. H.: 3D printed "smart screw" with built-in LC sensing circuit for wireless monitoring. In 19th International Conference on Solid-State Sensors. Actuators and Microsystems IEEE. (2017)
8. So, J. H., Thelen, J., Qusba, A., Hayes, G. J., Lazzi, G., Dickey, M. D.: Reversibly Deformable and Mechanically Tunable Fluidic Antennas. Adv. Funct. Mater. 19, 3632–3637 (2010)
9. Kimionis, J., Isakov, M., Koh, B. S., Georgiadis,A., Tentzeris, M. M.: 3D-Printed Origami Packaging With Inkjet-Printed Antennas for RF Harvesting Sensors. IEEE Transactions on Microwave Theory & Techniques. 63, 4521–4532 (2015)
10. Bharambe, V., Parekh, D. P., Ladd, C., Moussa, K., Dickey, M. D., Adams, J. J.: Vacuum-filling of liquid metals for 3D printed RF antennas. Addit Manuf. 18, 221–227 (2017)
11. Tang, X., Miao, Y., Chen, X., Nie, B.: A Flexible and Highly Sensitive Inductive Pressure Sensor Array Based on Ferrite Films. Sensors. 19, 2406 (2019)

12. Ota, H., Emaminejad, S., Gao, Y., Zhao, A., Wu, E., Challa, S., Chen, K., Fahad, H. M., Jha, A. K., Kiriya, D.: Application of 3D Printing for Smart Objects with Embedded Electronic Sensors and Systems. Adv. Mater. Technol. 1 (2016)
13. Ye, S., Feng, S., Huang, L., Bian, S.: Recent Progress in Wearable Biosensors: From Healthcare Monitoring to Sports Analytics. Biosensors. 10, 205 (2020)
14. Liu, H., Zhang, H., Han, W., Lin, H., Li, R., Zhu, J., Huang, W.: 3D Printed Flexible Strain Sensors: From Printing to Devices and Signals. Adv.Mater. 33 (2021)
15. Rafat, S., Maximilian, B., Wolfgang, E., André, Z.: Bending Setups for Reliability Investigation of Flexible Electronics. Micromachines. 12 (2021)
16. Vatani, M., Lu, Y., Engeberg, E. D., Choi, J. W.: Combined 3D printing technologies and material for fabrication of tactile sensors. Int J Precis Eng Man. 16, 1375–1383 (2015)
17. Sevval, C. M., Aylin, K. T. H.: Flexible electronics from hybrid nanocomposites and their application as piezoresistive strain sensors. Compos. B. Eng. 224 (2021)
18. Kim, H., Gibson, J., Maeng, J., Saed, M. O., Ware, T. H.: Responsive, 3D Electronics Enabled by Liquid Crystal Elastomer Substrates. ACS APPL MATER INTER. (2019)
19. Liu, S., Shi, X., Li, X., Sun, Y., Zhu, J., Pei, Q., Liang, J.: A general gelation strategy for 1D nanowires: dynamically stable functional gels for 3D printing flexible electronics. Nanoscale. (2018)
20. Baek, S., Kwon, J., Mano, T., Tokito, S, Jung, S.: A Flexible 3D Organic Preamplifier for a Lactate Sensor. Macromol. Biosci. 20 (2020)
21. Lee, S. K., Oh, Y. C., Kim, J. H.: Fused Deposition Modeling 3D Printing-based Flexible Bending Sensor. *KSMPE.* 19, 63–71 (2020)
22. Bogue, R.: 3D printing: an emerging technology for sensor fabrication. SENSOR REV. 36, 333–338 (2016)
23. Muth, J. T., Vogt, D. M., Truby, R. L., Menguec, Y., Kolesky, D. B., Wood, R. J., Lewis, J. A.: Embedded 3D printing of strain sensors within highly stretchable elastomers. Adv. Mater. 26, 6307–6312 (2014)
24. Lazarus, N., Bedair, S. S., Smith, G. L.: Creating 3D printed magnetic devices with ferrofluids and liquid metals. Addit Manuf. 26, 15–21 (2019)
25. Lazarus, N., Meyer, C. D.: Stretchable inductor with liquid magnetic core. Mater. Res. Express. 3, 036103 (2016)
26. Li, L., Nassab, R. A., Yellen, B. B.: Monolithically integrated Helmholtz coils by 3-dimensional printing. Appl. Phys. Lett. 104, 190 (2014)
27. Wang, X., Jing, L.: Recent Advancements in Liquid Metal Flexible Printed Electronics: Properties, Technologies, and Applications. Micromachines. 7, 206 (2016)
28. Zhou, L., Fu, J., Gao, Q., Zhao, P., He, Y.: All-Printed Flexible and Stretchable Electronics with Pressing or Freezing Activatable Liquid-Metal-Silicone Inks. Adv. Funct. Mater. 30 (2020)
29. Farizhandi, A. A. K., Khalajabadi, S. Z., Krishnadoss, V., Noshadi, I.: Synthesized biocompatible and conductive ink for 3D printing of flexible electronics. J Mech Behav Biomed Mater. 110 (2020)

30. Ketterl, T. P., Vega, Y., Arnal, N. C., Stratton, J. W. I.: A 2.45 GHz phased array antenna unit cell fabricated using 3-D multi-layer direct digital manufacturing. Microw. Theory Tech. 63, 4382–4394 (2015)
31. Swensen, J. P., Odhner, L. U., Araki, B., Dollar, A.M.: Printing three-dimensional electrical traces in additive manufactured parts for injection of low melting temperature metals. J. Mech. Robot. 7, 021004 (2015)
32. Qin, P., Huang, G., Liang, J., Wang, Q., Deng, Z.: A Gravity-Triggered Liquid Metal Patch Antenna with Reconfigurable Frequency. Micromachines. 12 (2021)
33. Mohammed, A. M. S. S. D., Yin, Y.: Flexible Circular Polarized Monopole Antenna Using EGaIn Alloy and PDMS Material. ICJE. 6 (2020)
34. Cho, G., Park, Y.: Soft Gripper with EGaIn Soft Sensor for Detecting Grasp Status. Appl. Sci. 11 (2021)
35. Joshipura, I. D., Ayers, H. R., Castillo, G. A., Ladd, C., Tabor, C. E., Adams, J. J., Dickey, M. D.: Patterning and Reversible Actuation of Liquid Gallium Alloys by Preventing Adhesion on Rough Surfaces. ACS APPL MATER INTER. 24, 575–581 (2018)
36. Jeong, Y. R., Kim, J., Xie, Z., Xue, Y., Won, S., Lee, G., Jin, S., Hong, S., Feng, X., Huang, Y., Rogers, J. A., Ha, J.: A skin-attachable, stretchable integrated system based on liquid GaInSn for wireless human motion monitoring with multi-site sensing capabilities. NPG Asia Mater. 9 (2017)
37. Huang, Y., Mao, Z., Wang, Y., Zhao, Y.: A High-Q On-Chip Spiral Inductor Using Thick Copper Technology. Microelectronics. 43, 850–854 (2013)
38. Zeng, S., Chen, Z., Li, M.: A Ultra-thick Copper Based Inductor Using Single Damascene Process. Application of IC. 35, 51–54 (2018)
39. Wu, X., Shao, S., Chen, Z., Cui, Z.: Printed highly conductive Cu films with strong adhesion enabled by low-energy photonic sintering on low-Tg flexible plastic substrate. Nanotechnology. 28 (2017)
40. Zhang, Y., Li, N., Xiang, Y., Wang, D., Zhang, P., Wang, Y., Lu, S., Xu, R., Zhao, J.: A flexible non-enzymatic glucose sensor based on copper nanoparticles anchored on laser-induced graphene. Carbon. 156 (2020)
41. Rizwan, M., Kutty, A. A., Kgwadi, M., Drysdale, T. D., Sydanheimo, L., Ukonen, L., Virkki, J.: Possibilities of Fabricating Copper-Based RFID Tags With Photonic-Sintered Inkjet Printing and Thermal Transfer Printing. In IEEE ANTENN WIREL PR. 16, 1828–1831 (2017)
42. Yu, X., Mahajan, B. K., Shou, W., Pan, H., Ko, S., Lee, D., Wu, Z.: Materials, Mechanics, and Patterning Techniques for Elastomer-Based Stretchable Conductors. Micromachines. 8 (2016)
43. Lee, P., Ham, J., Hong, S., Han, S., Suh, Y. D., Lee, S. E., Yeo, J., Lee, S. S., Lee, D.: Highly stretchable or transparent conductor fabrication by a hierarchical multiscale hybrid nanocomposite. Adv. Funct. Mater. 24, 5671–5678 (2014)

Figures

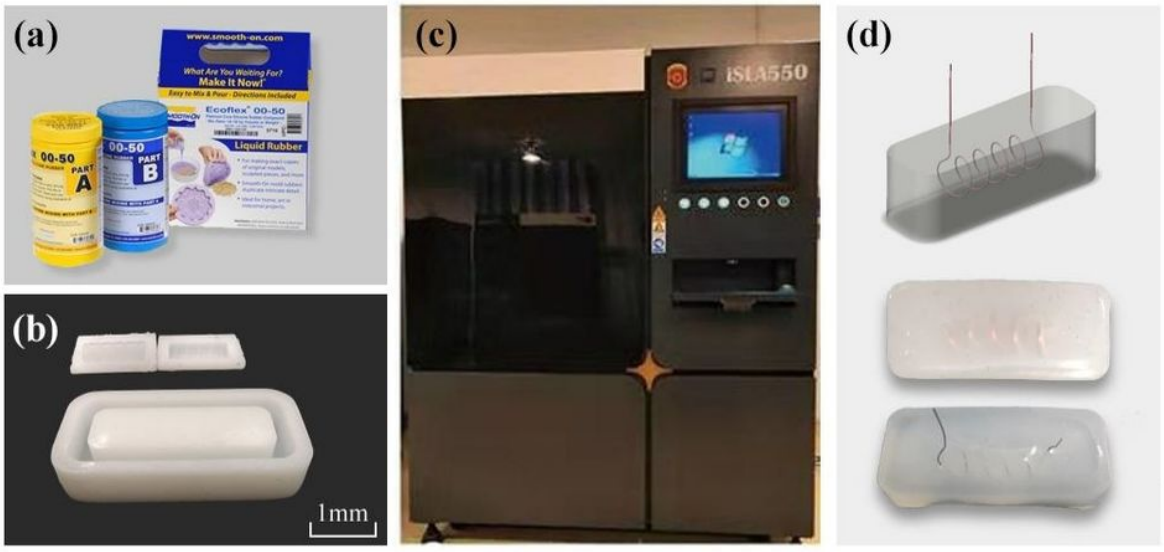

Figure 1

Preparation materials and equipment for flexible microspiral inductor: (a) Ecoflex 00-50 material manufactured by BASF, Germany; (b) 3D-printed mold made of photosensitive resin; (c) Z Rapid SL500 light curing 3D printer; (d) (top) Theoretical model and (bottom) actual samples of microspiral inductor.

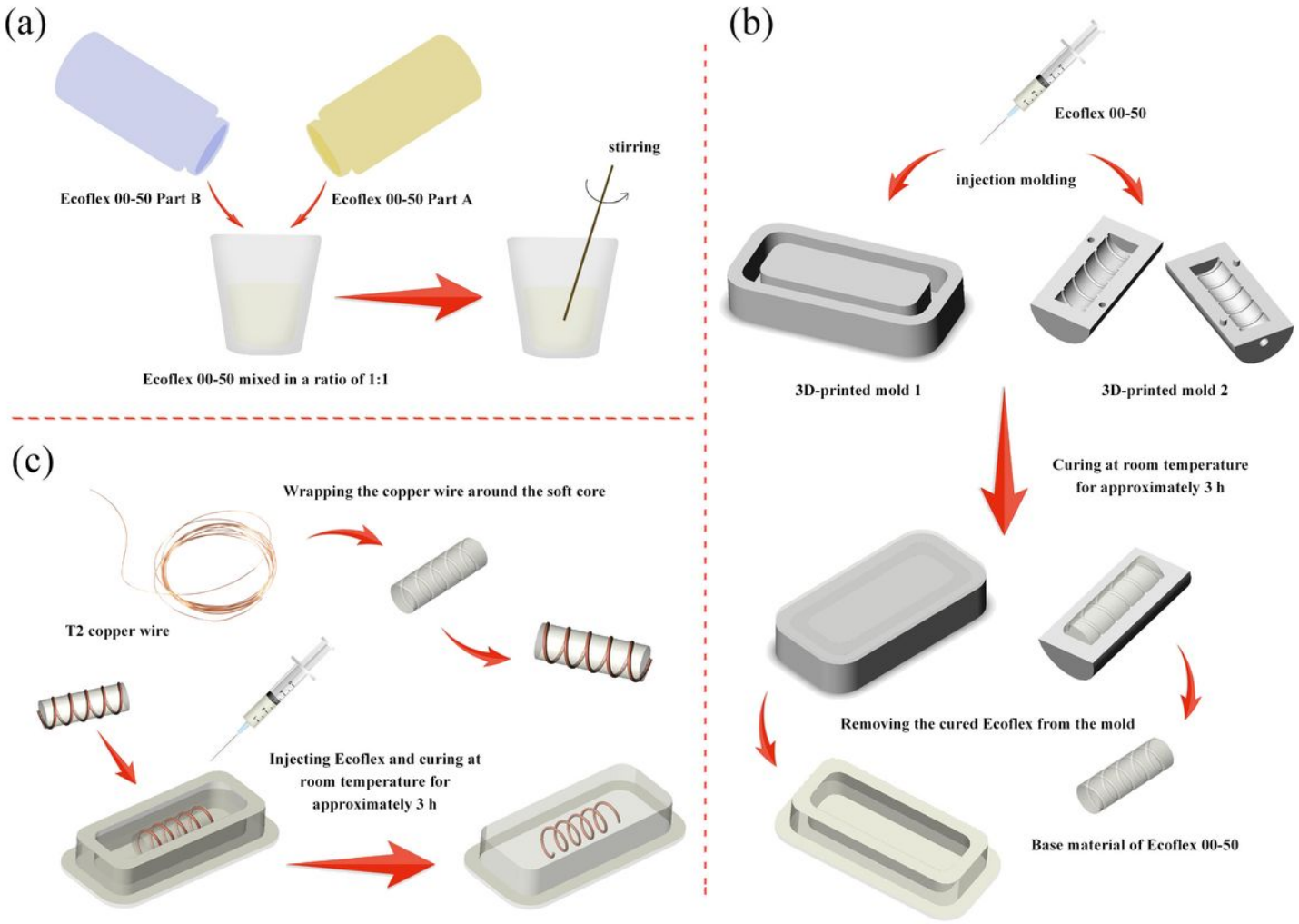

Figure 2

Preparation process of flexible microspiral inductor: (a) Mix Ecoflex 00-50 and stir evenly; (b) Ecoflex is injected into a 3D-printed mold and cured at room temperature; (c) Copper wire is wound on the soft core, and Ecoflex is injected and cured at room temperature.

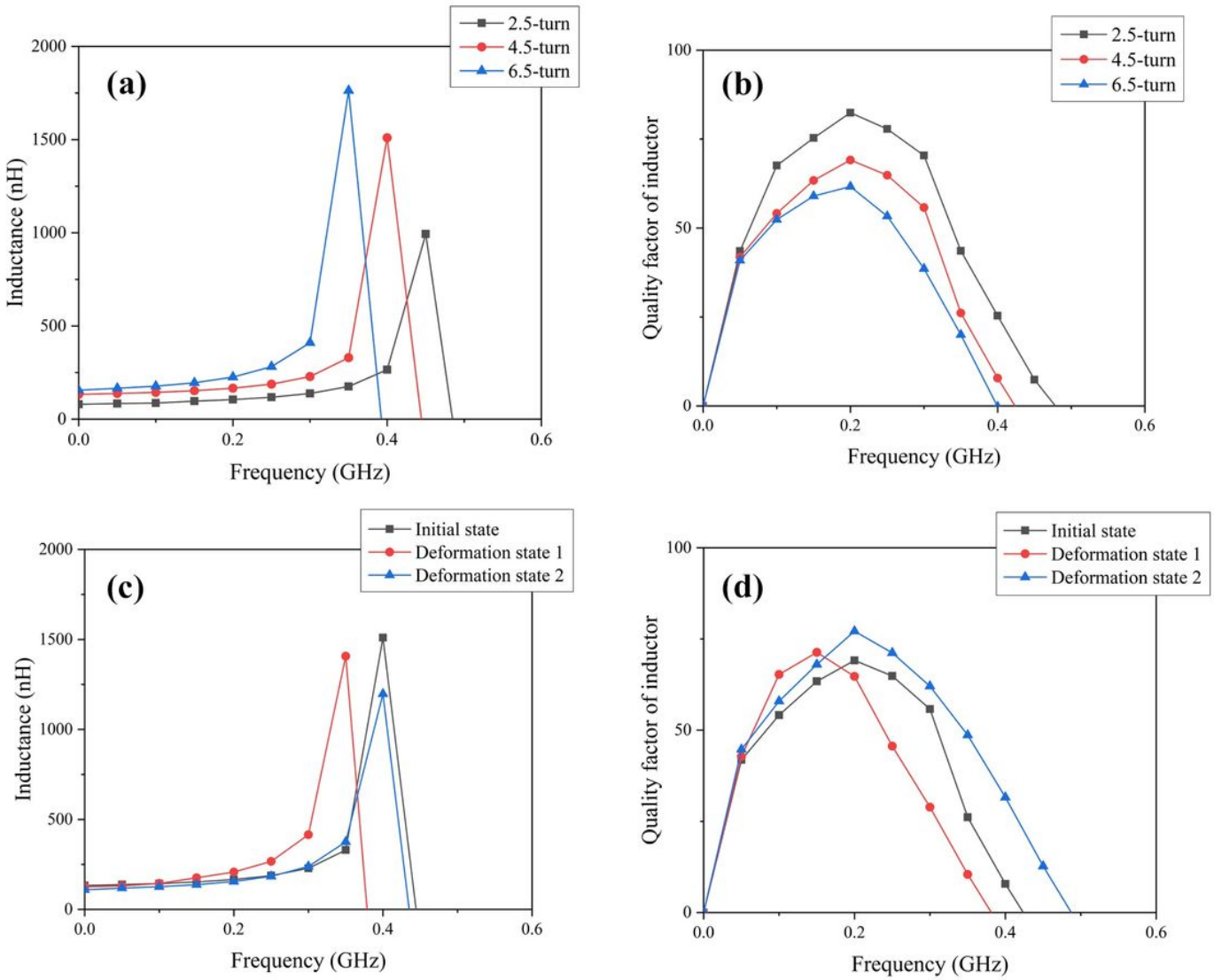

Figure 3

Line chart of the numerical simulation results of a flexible microspiral inductor: (a) Simulation results of the inductance and (b) quality factor Q of microspiral inductors with 2.5, 4.5, and 6.5 turns; (c) Simulation results of the inductance and (d) quality factor Q of the 4.5-turn microspiral inductor under deformation.

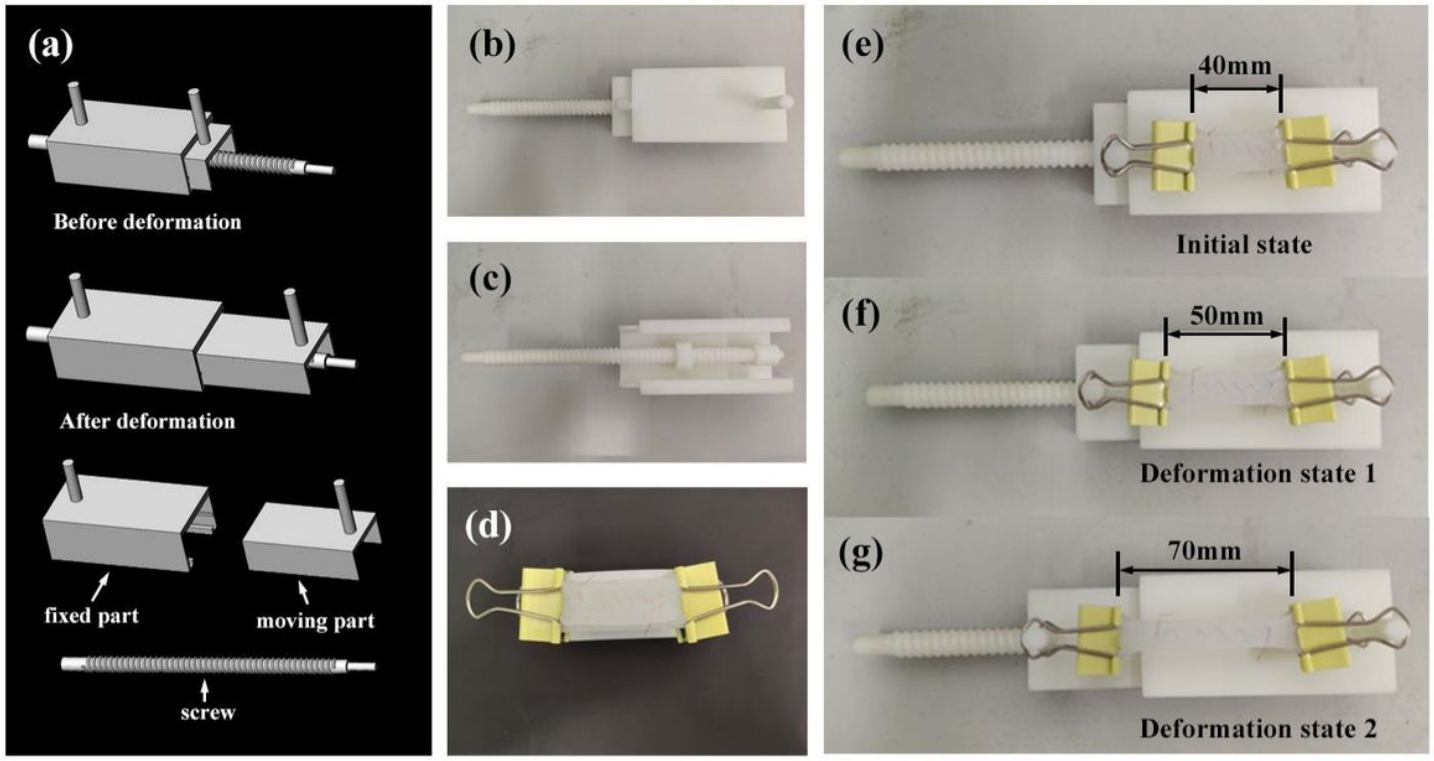

Figure 4

SolidWorks model of a tensile deformation fixture and 3D-printed physical model: (a) SolidWorks model of the fixture and its components; (b) Top view of the fixture; (c) Bottom view of the fixture; (d) Flexible microspiral inductor fixed by two clips; (e) Initial state of the flexible microspiral inductor placed on the fixture; (f) Microspiral inductor tensile deformation state 1; (g) Microspiral inductor tensile deformation state 2.

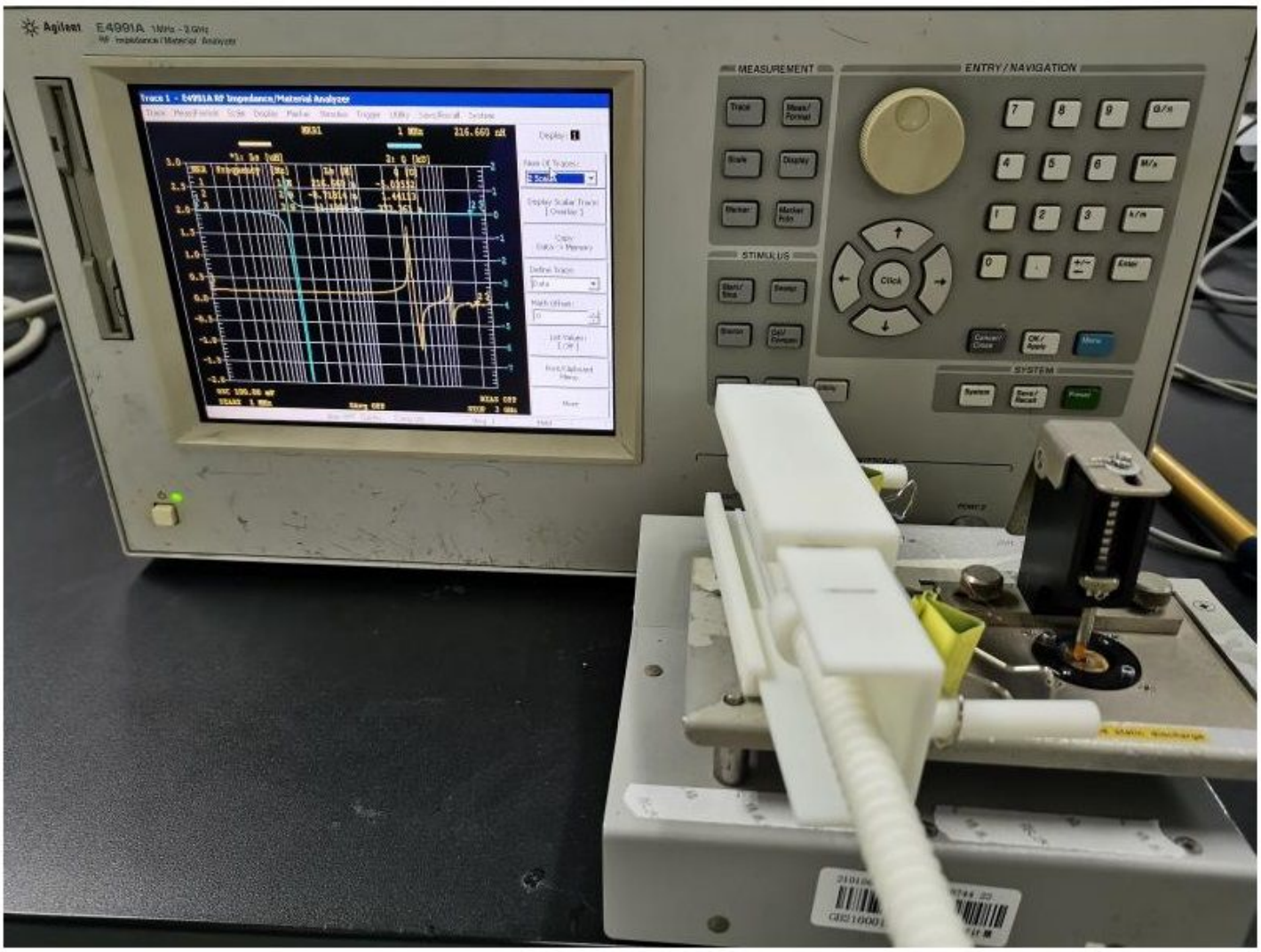

Figure 5

Agilent E4991A impedance analyzer

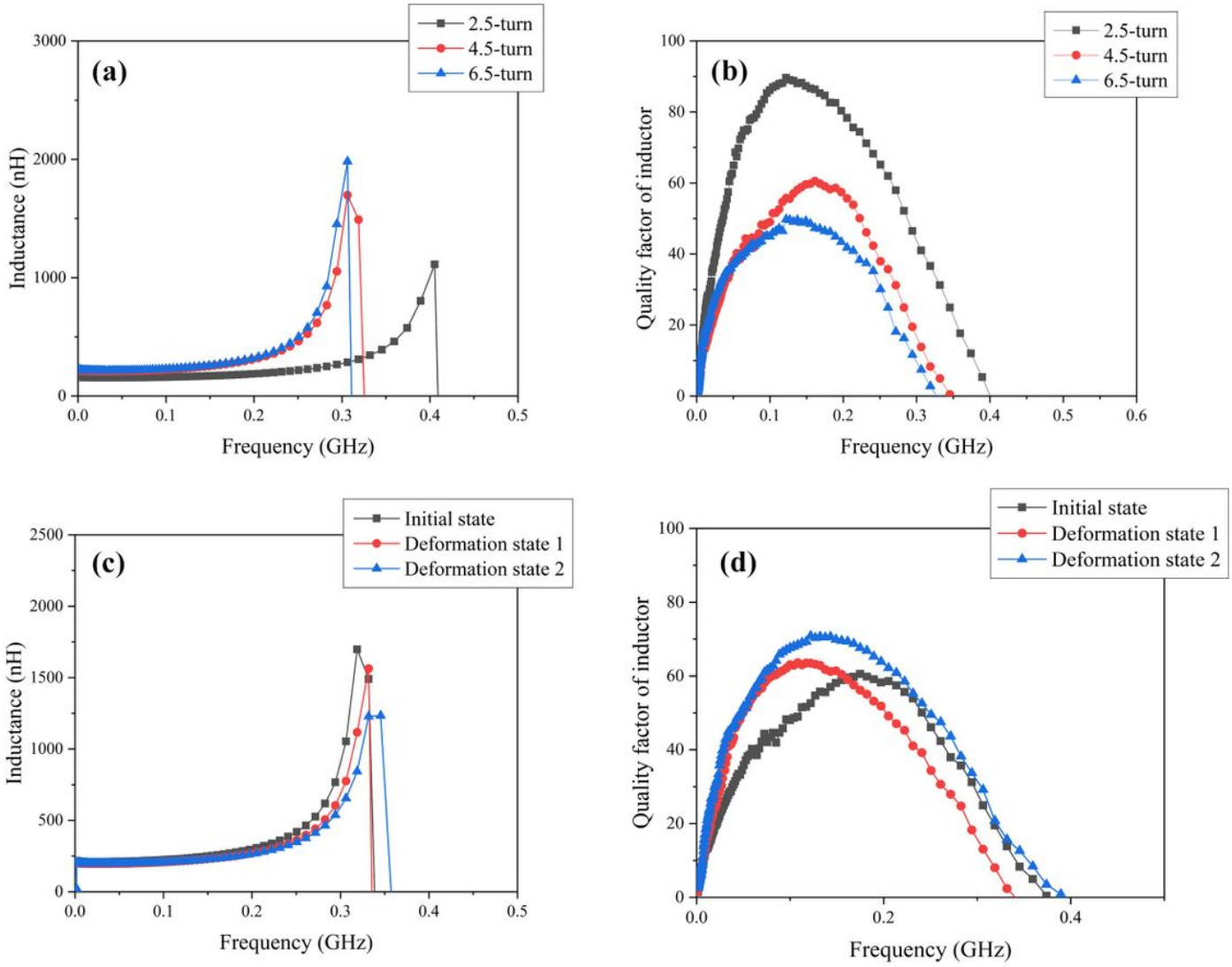

Figure 6

Line chart of the electrical test results of the flexible microspiral inductor: (a) Test results of inductance and (b) quality factor Q of microspiral inductors with 2.5, 4.5, and 6.5 turns; (c) Test results of inductance and (d) quality factor Q under deformation of the 4.5-turn microspiral inductor.

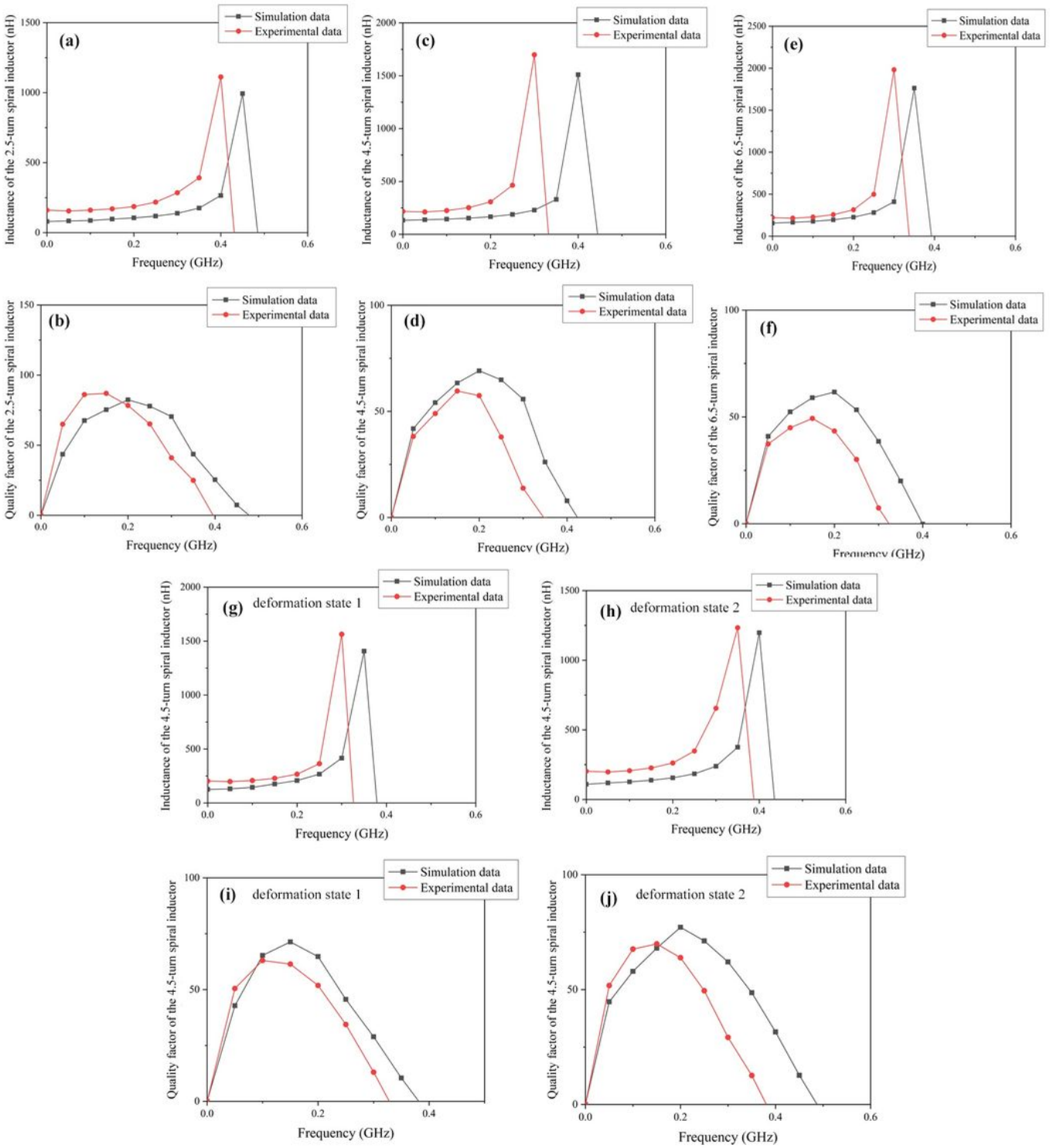

Figure 7

Comparison between the numerical simulation results and physical experiment results of the flexible microspiral inductor: (a) Comparison between the inductance and (b) quality factor Q of the 2.5-turn microspiral inductor; (c) Comparison between the inductance and (d) quality factor Q of the 4.5-turn microspiral inductor; (e) Comparison between the inductance and (f) quality factor Q of the 6.5-turn microspiral inductor; (g) Comparison between the inductance and (h) quality factor Q in deformation

state 1 of the 4.5-turn microspiral inductance; (i) Comparison between the inductance and (j) quality factor Q in the deformation state 2 of the 4.5-turn microspiral inductance.